Generalizing, Extending, and Maximizing Nitrogen-15 Hyperpolarization Induced by Parahydrogen in Reversible Exchange

Johannes F. P. Colell,[†] Angus W. J. Logan,[†] Zijian Zhou,[†] Roman V. Shchepin,[‡] Danila A. Barskiy,[‡] Gerardo X. Ortiz, Jr.,[†] Qiu Wang,[†] Steven J. Malcolmson,[†] Eduard Y. Chekmenev,[‡,§] Warren S. Warren,*,[†,∥] and Thomas Theis*,[†]

[†]Department of Chemistry, Duke University, Durham, North Carolina 27708, United States

[‡]Vanderbilt University Institute of Imaging Science (VUIIS), Department of Radiology, Department of Biomedical Engineering, Vanderbilt Ingram Cancer Center (VICC), Vanderbilt University, Nashville, Tennessee 37232, United States

[§]Russian Academy of Sciences, Moscow, Russia

[∥]Departments of Physics, Radiology and Biomedical Engineering, Duke University, Durham, North Carolina 27707, United States

S *Supporting Information*

ABSTRACT: Signal Amplification by Reversible Exchange (SABRE) is a fast and convenient NMR hyperpolarization method that uses cheap and readily available *para*-hydrogen as a hyperpolarization source. SABRE can hyperpolarize protons and heteronuclei. Here we focus on the heteronuclear variant introduced as SABRE-SHEATH (SABRE in SHield Enables Alignment Transfer to Heteronuclei) and nitrogen-15 targets in particular. We show that ^{15}N-SABRE works more efficiently and on a wider range of substrates than ^{1}H-SABRE, greatly generalizing the SABRE approach. In addition, we show that nitrogen-15 offers significantly extended T_1 times of up to 12 minutes. Long T_1 times enable higher hyperpolarization levels but also hold the promise of hyperpolarized molecular imaging for several tens of minutes. Detailed characterization and optimization are presented, leading to nitrogen-15 polarization levels in excess of 10% on several compounds.
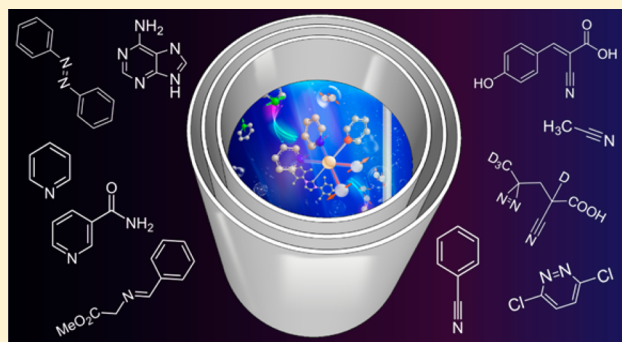
INTRODUCTION

Hyperpolarization techniques enhance nuclear polarization and nuclear magnetic resonance (NMR) signals by 4 to 8 orders of magnitude.[1−11] The concomitant increase of signal-to-noise (S/N) has opened new opportunities for *in vitro* NMR studies such as nanomolar detection[12−15] and *in vivo* MRI with direct access to metabolic activity on the molecular level.[16−20]

Signal Amplification By Reversible Exchange (SABRE)[21] is the nonhydrogenative variant of *para*-hydrogen induced polarization (PHIP).[22−25] A hydrogenation reaction is not required, and substrates can be hyperpolarized continuously or repeatedly. Furthermore, SABRE occurs in the liquid state at room temperature and requires only inexpensive equipment.[21,26,27] As depicted in Scheme 1, SABRE uses a transition metal catalyst to establish contact between the polarization source, *para*-H$_2$, and the target nuclei.

Specifically, magnetic contact is established by the *J*-coupling of the *para*-H$_2$-derived hydrides to the target nuclei across the iridium center. Reversible exchange of hydrides and substrate leads to continuous hyperpolarization buildup on the substrate as long as fresh *para*-H$_2$ is supplied. Accordingly, SABRE has also been referred to as polarization transfer catalysis (PTC).[28]

Scheme 1. Reversible Exchange of *para*-H$_2$ and Substrate on the Polarization Transfer Catalyst Leads to Continuous Buildup of Polarization on the Free Substrate[a]
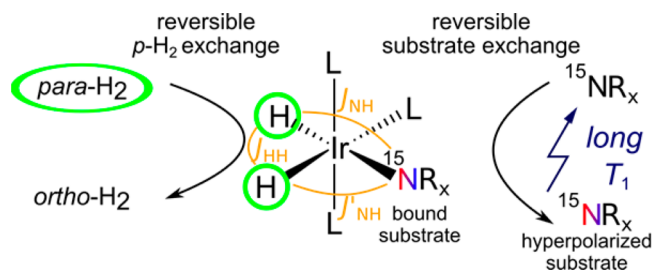
[a]The *J*-couplings in the polarization transfer complex drive the polarization transfer. L: Ligands. Rx: arbitrary group.

Until recently, SABRE was primarily focused on ^{1}H nuclei, where T_1 is typically short (several seconds), and high ^{1}H polarization levels (1%) are observed predominantly for Lewis

basic *N*-heterocyclic molecules. On the other hand, hetero-nuclei (e.g., ^{15}N, ^{13}C, ^{31}P) offer long T_1 relaxation times, in particular at low magnetic fields, and allow for large polarization levels for a wider variety of structural motifs. As demonstrated recently, heteronuclei are most efficiently targeted when conducting SABRE at magnetic fields of a few μT inside magnetically shielded environments (SABRE-SHEATH).[29−31] Here we focus on the direct hyperpolarization of nitrogen-15 at μT magnetic evolution fields. The relatively simple experimental procedure is shown in the Supporting Information video.

The present contribution presents three major points. First, we demonstrate that the substrate scope is significantly expanded with SABRE-SHEATH. This is because nitrogen is directly bound to iridium, unlike the protons in the R-groups. Second, we show that long T_1 lifetimes, in excess of 10 min, can be obtained at relatively low fields in 1 T permanent magnets. This is significant because the combination of low cost hyperpolarization with low cost NMR detection sets the stage for affordable and highly sensitive NMR spectroscopy and molecular magnetic resonance imaging (MRI). Lastly, we optimize the SABRE-SHEATH process in detail leading to nitrogen-15 hyperpolarization in excess of 10%.
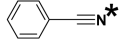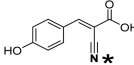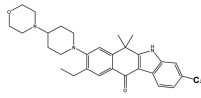
■ METHODS
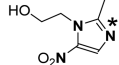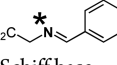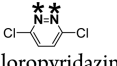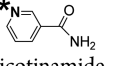
Methanol-d_4 solutions with defined concentrations of precatalyst ([IrCl(COD)(IMes)]; COD = 1,5-cyclooctadiene; IMes = 1,3-bis(2,4,6-trimethylphenyl)-imidazol-2-ylidene, substrate (Sub), and coligand (L) were converted to catalytically active solutions of ([Ir(H)$_2$(IMes)L$_x$Sub$_{3-x}$]) by bubbling hydrogen gas through these solutions. The pressure was regulated to 10 bar. The pressure gradient across the sample was negligible (<0.1 bar), just enough to establish the desired flow rate (typically 60 sccm ≈ 6 ccm at 10 bar). The flow rate is set with a needle valve at the outlet after the bubbling stage, directly venting the hydrogen gas into a hood.

The sample volume was 500 μL inside a medium-walled 5 mm pressure NMR tube (Wilmad 524-PV-8). The *para*-H$_2$ fraction was 80−90% unless noted otherwise. After a suitable activation period (10 min to 1 h), samples were placed in a defined magnetic evolution field B_{evo} in the μT range. Evolution time in the shield exceeded the build-up time to yield maximal signal intensity. The T_1 measurements were performed from a single hyperpolarization proces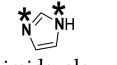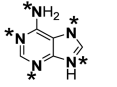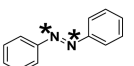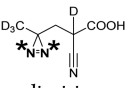s by a sequence of small tip angle (6°) pulses. Measurements at 1 T were performed in a benchtop NMR instrument (Magritek 15N-Spinsolve). Measurements at 8.45 T were carried out on a Bruker Avance DX360 NMR spectrometer. See Supporting Information (SI) for additional experimental details, a theoretical model of SABRE-SHEATH, as well as a video illustrating experiments.

■ RESULTS AND DISCUSSION

I. Expansion of Substrate Range. The generalized substrate scope is illustrated in Table 1. (Full experimental details are provided in the SI). The results suggest that, in general, sp and sp²-hybridized ^{15}N sites can be hyperpolarized. This is significant because sp and sp² hybridized nitrogens are found in a wide range of metabolites and drugs.[32] It is noteworthy that ^1H enhancements are negligible, except for Entries 5 and 8, formally imidazole and pyridine derivatives. Table 1 includes T_1 values, where available; however, they vary

Table 1. ^{15}N-SABRE-SHEATH Enhancements (ε) over Thermal Measurements at 8.5 T, Polarization Levels, and T_1 in Methanol-d_4 for Diverse Molecular Motifs[d]

Entry	Substrate	ε	P [%]	T_1 [min]
1	acetonitrile	4,400	1.3	3.5 @ 1 T
2	benzonitrile	21,000	6.8	12 @ 1 T
3	CHCA	3,600	1.1	1.2 @ 1 T in D2O
4	alectinib	5,000	1.5	N/A
5	metronidazole	72,000	24	0.6 @ 9.4 T
6	Schiff base	7,200	2.1	2.2 @ 1 T
7	dichloropyridazine	12,000	3.5	0.25 T$_S$: 0.6 @8.5 T
8	nicotinamide	11,000[a]	3.4	2.1 @ 1 T in D2O
9	imidazole	2,000[a]	0.58[a]	0.4 @9.4 T
10	adenine	200[b]	0.06	N/A
11	diphenyldiazene	> 40[c]	>0.01	0.15 T$_S$: 1 @ 8.5 T
12	diazirine	15,000	4.4	5 T$_S$: 23 @0.3 mT

[a]Data obtained with 50% *para*-H2. [b]Enhancements averaged over all ^{15}N sites. [c]SABRE hyperpolarizes the *Z*-isomer. See SI for additional information. [d]* indicates hyperpolarized site.

strongly with concentration, solvent, and magnetic field (see below).

The first four entries are nitriles (sp-hybrid ^{15}N), commonly encountered in biologically active molecules and drugs.[32] Nitriles have been reported as ^{1}H-SABRE substrates, but enhancements did not exceed ∼60-fold (over 9.4 T).[33] In contrast, with SABRE-SHEATH, nitriles consistently show polarization levels of several percent (see Table 1). Nitriles are particularly versatile; polarization levels remain large irrespec-

Table 2. Comparison of Spin−Lattice Relaxation Times T_1 and Signal-to-Noise in a Single 90°-Acquired Experiment of Dilute (Methanol-d_4) and Neat Solutions at 8.5 and 1 T[a]

compound	conc. [mM]	T_1 @ 8.5 T [min]	T_1 @ 1 T [min]	S/N @ 8.5 T	S/N @ 1 T
^{15}N-pyridine	50	1.05 ± 0.02	2.06 ± 0.13	5700	1500
^{15}N-acetonitrile	50	2.05 ± 0.02	3.73 ± 0.05	5000	2900
^{15}N-benzonitrile	50	2.15 ± 0.02	11.95 ± 0.35	7300	1400
^{15}N$_2$-diazirine	50	0.16 ± 0.002	4.35 ± 0.1	1200	1300
pyridine	neat (12.4 M)	1.5 ± 0.05	3.31 ± 0.3	300	300
pyridine-d_5	neat (12.4 M)	1.6 ± 0.02	3.68 ± 0.45	1300	400
acetonitrile	neat (19.1 M)	2.2 ± 0.05	2.3 ± 0.4	1000	200
acetonitrile-d_3	neat (19.1 M)	2.36 ± 0.03	2.01 ± 0.1	1900	400
benzonitrile	neat (9.7 M)	2.88 ± 0.03	10.5 ± 1	7100	2600

[a]Neat solutions have ^{15}N at natural abundance (0.36%).

tive of the backbone structure or system composition. Many substituents, including unsaturated bonds, hydroxyl and carboxylic acid groups are tolerated. Examples are α-cyano-4-hydroxycinnamic acid (CHCA, entry 3) with potentiating effects for chemotherapy[34] and alectinib (entry 4), a potent inhibitor of anaplastic lymphoma kinase (ALK) also used for the treatment of nonsmall cell lung cancer.

The remaining entries in Table 1 (entries 6−12) all contain sp^2-hybridized ^{15}N. As a first example, metronidazole (entry 5) is an antibiotic also used as a hypoxia probe.[35−39] Very high polarization levels are observed for this molecule, when nitrogen is at its natural abundance of 0.36%. Next, we found that ^{15}N nuclei in a wide range of Schiff bases (entry 6), which included biologically relevant scaffolds, such as pyridoxal phosphate analogues and retinal with critical roles in visual signaling, hyperpolarize well.[40−42]

Dichloropyridazine (entry 7) also illustrates the basic principle: the ^{15}N sites hyperpolarize well, whereas the protons do not because they do not directly interact with the catalyst. This molecule also is the first example with two adjacent ^{15}N nuclei, offering the opportunity to store hyperpolarization in long-lived singlet states characterized by extended decay time constants T_S.[43]

A further interesting substrate is nicotinamide (vitamin B$_3$, entry 8) with its important functions in mammalian metabolism.[44−47] A significant opportunity in current medical imaging is presented by imidazole (entry 9) which has a pK_A of ∼7.1, ideal for *in vivo* pH sensing.[48] Furthermore, nucleobases, such as adenine (entry 10), are also amendable to hyperpolarization. Surprisingly, enhancements can be detected for all nitrogen positions including the amino group, presumably due to the existence of the enamine−imine tautomer, which is structurally similar to Schiff bases (or indirect polarization transfer). Diphenyldiazene (entry 11) exhibits E/Z isomerism induced optically,[49,50] or chemically.[51] Interestingly the Z form is hyperpolarized exclusively despite the fact that the E form is thermodynamically stable. Enhancements of the Z-form, in presently unknown low concentration, significantly exceed 40-fold (see SI). The last entry, a diazirine (entry 12), stands out as it offers particularly long decay time constants, T_1 of 5 min and T_S of above 20 min, allowing for detection of enhanced signal for hours after polarization buildup. These diazirine moieties can readily be incorporated in a wide range of drugs or biomolecules replacing CH$_2$− groups.[52]

The lowest enhancements are recorded for imidazole (entry 9)[48] and adenine (entry 10) with exchanging protons at the ^{15}N sites. This causes shorter T_1 times and significant polarization losses during transfer to the detection field (∼8 s in our

experiments). For substrates with exchanging protons higher pH values are associated with larger enhancements because deprotonated forms bind to the catalyst more easily and because T_1 is longer on deprotonated ^{15}N.

II. Extended Relaxation Times. Nitrogen-15 SABRE is particularly appealing because many substrates show large T_1 times, which enables the observation of slow processes, such as diffusion, biochemical reactions, or downstream metabolic processes. Table 2 lists T_1 times and S/N (signal-to-noise) for various substrates at two different magnetic fields, 8.5 and 1 T. Measurements at 1 T were performed in an inexpensive, portable benchtop NMR instrument (Magritek 15N-Spinsolve), illustrating the potential of low-cost high-sensitivity NMR when combining SABRE hyperpolarization with permanent magnet-based technology. Since most clinical MRI scanners operate in the 1−3 T range, measurements at 1 T are useful for future biomedical translation.

The results clearly show that T_1 times strongly depend on the magnetic field and molecular structure. The molecular environment of the respective spin determines which relaxation mechanism is relevant. Usually, NMR relaxation is dominated by dipolar relaxation, caused by other nearby spins, and has a relatively weak field dependence. However, nitrogen-15, which is often far removed from other spins, can be dominated by chemical shift anisotropy (CSA) relaxation. Under these circumstances a strong field dependence is expected because CSA relaxation scales with B_0^2.[53]

This is best exemplified by ^{15}N-benzonitrile and ^{15}N$_2$-diazirine. In benzonitrile dipolar relaxation is minimized, as protons are far away from the nitrogen nucleus. We observe $T_1 \approx 2.15$ min at 8.5 T and $T_1 \approx 11.95$ min at 1 T; CSA dominates relaxation. In the ^{15}N$_2$-diazirine the field dependence is even more pronounced. At 8.5 T we measure T_1 of ∼10 s, but at 1 T, $T_1 \approx 4.35$ min. Note that we recently also reported the relaxation time constant of the long-lived singlet state in diazirine with T_S in excess of 20 min at $B_0 = 0.3$ mT.[52]

Now we focus our attention on the S/N comparison between the investigated magnetic fields. In NMR with thermally polarized spins, signal scales with B_0^2, as, both, polarization and induction are proportional to B_0.[53,54]

The noise, on the other hand (in the coil noise dominated regime), scales with $B_0^{1/4}$; hence S/N scales with $B_0^{7/4}$.[54−56] However, if the polarization source is an external hyperpolarizer, spin polarization is no longer determined by B_0 and S/N scales as $B_0^{3/4}$. The expected signal loss in our experiments when going from 8.5 to 1 T is thus $(8.5/1)^{3/4} \approx 5$. However, it is evident from Table 2 that measurements at 1 T are on average only 2.8 times less sensitive than at 8.5 T. This can be

attributed to different pickup-coil design, where coil sensitivity is higher at 1 T as the inductance in solenoid coils (used at 1 T) is larger than in saddle coils (used at 8.5 T).[57] An additional factor is relaxation during sample transfer from the hyperpolarization region to detection fields (~1 s to 1 T, ~8 s to 8.5 T). The latter effect is best exemplified by the molecule with the most pronounced field dependence of the relaxation time ($^{15}N_2$ diazirine). In this case, the S/N is better at 1 T than at 8.5 T because of reduced relaxation losses in 1 T experiments. Notice that the S/N comparisons were performed without additional delays before acquisition. With additional delays, the low-field experiments would be more favorable because of extended T_1.

For future applications, an important scenario is body-noise-dominated magnetic resonance, as is the case for human MRI. Here body-noise (dielectric loss) dominates, and the S/N with thermal magnetization is proportional to B_0.[55,58] Accordingly, for hyperpolarized MRI, S/N is expected to be directly proportional to hyperpolarization level and independent of B_0.[57,59] Therefore, NMR and MRI in low fields are of great general interest as magnet and RF-circuit design is more flexible, and devices are portable and relatively cheap.[59,60] For example, recent advances in low-field MRI have already enabled high performance ^1H-MRI at fields as low as 6.5 mT, even using thermal magnetization.[61] The newest advances, such as "External High-Quality-factor-Enhanced NMR" (EHQE-NMR)[62] and others,[63] lead to independence of B_0, even for spectroscopic applications of hyperpolarized MR.

Both the presented T_1 lifetime and S/N results suggest that NMR and MRI with hyperpolarized heteronuclei can benefit from low fields. Especially, the combination of a simple hyperpolarization technique like SABRE with low-field detection appears as a powerful approach. Costs go down, and relaxation times go up without sacrificing S/N. With SABRE-SHEATH, ^{15}N-labeled markers can be hyperpolarized continuously or repeatedly, directly in room-temperature solutions. Thus, low-field NMR and MRI with SABRE may enable high sensitivity NMR and MRI for a large audience at moderate cost with many applications.[64,65]

III. Analysis of Temperature and Field Dependence.

Enhancements and polarization levels reported in Table 1 are not optimized with respect to all variables affecting efficiency, i.e., catalyst and substrate concentrations, coligand concentration, para-H_2 pressure/flow rate, temperature, magnetic field, etc. The experimental efforts involved in globally optimizing this multidimensional parameter space would not be practicable for all substrates.

Here we focus on the dependence of polarization on magnetic evolution field B_{evo} and average complex lifetime τ_{life} using a suitable model system. This model system needs to exhibit large, stable enhancements over many experiments and have a relatively quick polarization buildup (<5 min), and continuous repetition of experiments must be possible. We use a system similar to Mewis et al.,[33] i.e., acetonitrile-15N (100 mM), IrCl(IMes) (COD) (5 mM), and pyridine (33 mM) in methanol-d_4. (Pyridine is added for stability; without this coligand experiments were inconsistent.) Note that ^1H enhancements did not exceed 60-fold (over thermal polarization at 9 T),[33] whereas ^{15}N exhibits more than 4000-fold enhancement. This particular system composition yields large S/N and long-term stability, not maximum ^{15}N-polarization (vide infra).
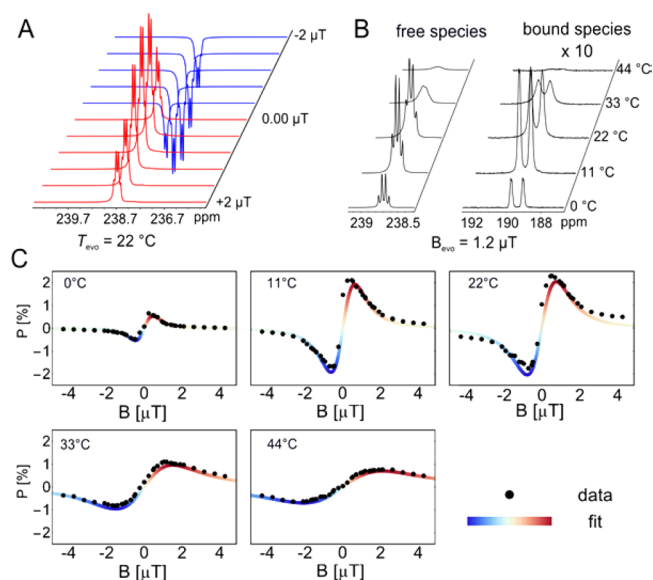

Figure 1. Temperature and field dependence of SABRE-SHEATH. (A) Excerpt of the experimental ^{15}N spectra at different magnetic evolution fields at a temperature of 22 °C. (B) NMR spectra at constant magnetic field but different temperatures. (C) Free substrate ^{15}N polarization at different magnetic evolution fields and temperatures. The data are fit to a simple theoretical model derived from the three-spin model as shown in Scheme 1 and Figure 2A. Red vs blue highlights the 180° phase shift.

In Figure 1 we show that ^{15}N polarization strongly depends on magnetic field (Figure 1A) and temperature during evolution in the shield (Figure 1B). We observe that the phase of the hyperpolarized signal (with respect to a fixed detector phase) can be controlled by the magnetic evolution field (i.e., 180° phase shift is observed upon B_{evo} inversion; see Figure 1, A and C). This is a useful feature for hyperpolarization experiments because it allows for simple difference measurements, as well as easy distinction of hyperpolarized signals from the thermal background. This inversion is associated with the existence of the two matching conditions.[66,67]

In the absence of chemical exchange we obtain

$$B_{evo} = \pm[J_{HH} + (J_{NH} + J'_{NH})/4]/(\gamma_H - \gamma_N) \qquad (1)$$

where the J coupling parameters are defined in Figure 2. The expected optimal field is $B_{evo} = \pm0.3$ μT. However, the experimental data from Figure 1C clearly show that the maxima are shifted to higher magnetic fields and scale with the temperature. These shifts are caused by broadening of the resonance conditions as a result of chemical exchange. Shorter catalyst/substrate complex lifetimes, at elevated temperatures, cause broader resonance conditions and more overlap. In the SI we develop a theory that includes the exchange and obtains an analytical expression that only depends on the J-coupling parameters, the magnetic field, and the average catalyst lifetime. We use this expression to fit the data as illustrated in Figure 1C and obtain excellent qualitative agreement; however, quantitative agreement with experimental lifetime is not obtained. Experimentally, it is easy to determine the J-couplings and the average lifetime τ_{life} as depicted in Figure 2B. Specifically, the substrate dissociation limited catalyst lifetime[68] is monitored by the change in NMR line width $\Delta\nu_i$ of the catalyst bound and free species[69]
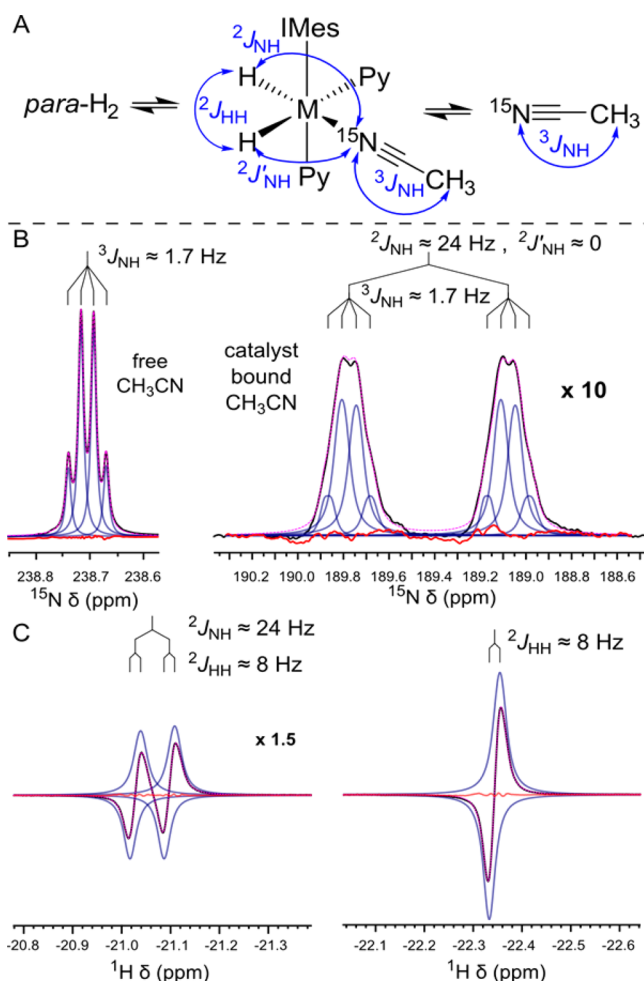
Figure 2. J-coupling and line width analysis. (A) Exchange between bound and free species (^{15}N−CH$_3$CN, H$_2$) and J-coupling definitions. (B) Lineshape analysis of ^{15}N spectra (blue: individual Lorentzians, black: experimental trace, pink: overall fit, red: residual error optimized to rms-noise level). (C) ^{1}H spectra of the hydride region taken under PASADENA conditions.[25]

$$\tau_{life} = 1/(\pi(\Delta\nu_{bound} - \Delta\nu_{free})) \qquad (2)$$

At the temperature corresponding to maximum enhancement (22 °C), we experimentally determine a lifetime of 44−46 ms. At low temperature of 0 °C line widths are small enough to determine relevant J-coupling constants ($^2J_{HH'}$ = 8 Hz, $^3J_{NH}$ = 1.71 Hz, $^3J_{NH,bound}$ = 1.69 Hz, ΔJ_{NH} = $^2J_{NH}$ − $^2J_{NH'}$ = 24 Hz). The couplings were used as fixed parameters to determine the individual line positions for evaluation of the line widths at higher temperatures. The experimental data also indicate that the major chemical species under our experimental conditions is indeed the system illustrated in Figure 2A because the nonequivalent hydrides indicate different ligands (pyridine and ^{15}N−CH$_3$CN) in the equatorial plane.

IV. Maximizing Polarization. After the above study of hyperpolarization as a function of temperature and magnetic field, further optimization requires inspection of concentrations of catalyst, substrate, and coligand, as well as para-H$_2$ pressure/flow rate. Here we performed a careful study to determine optimum catalyst concentration by conducting a dilution series at fixed catalyst loading (c_{sub}/c_{cat} = 20, see Figure 3A). We find maximum enhancement at 0.25 mM [IrCl(IMes)(COD)] and 5 mM ^{15}N−CH$_3$CN in the presence of 0.25 mM pyridine as

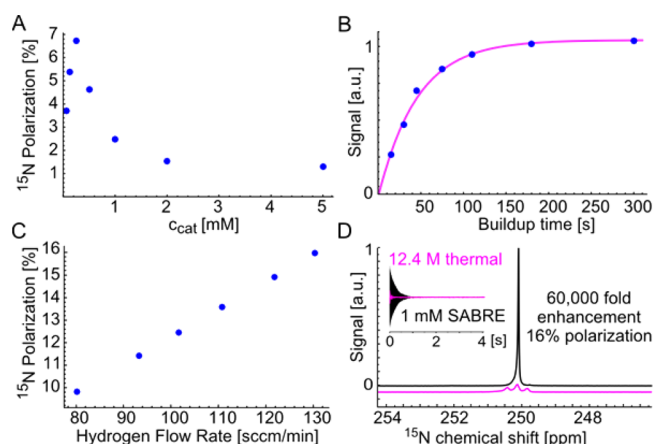Figure 3. (A) ^{15}N polarization of ^{15}N−CH$_3$CN as a function of the catalyst concentration at fixed catalyst loading of 5 mol%. (B) ^{15}N signal as a function of the buildup time (T_b = 40.8 s). (C) ^{15}N polarization as a function of the hydrogen flow rate ($c_{Catalyst}$ = 0.25 mM, $c_{Pyridine}$ = 0.25 mM, $c_{Benzonitrile}$ = 1 mM). (D) Comparison of a neat ^{15}N pyridine reference (c = 12.4 M, pink, thermal 8.45 T, shifted by 63 ppm) and ^{15}N spectrum of hyperpolarized benzonitrile (c = 1 mM, conditions as in C).

stabilizing coligand, corresponding to P_{15N} = 7% (enhancement of 23 000-fold at 8.5 T). It is noteworthy that the maximum polarization is observed at the same catalyst concentration experimentally determined for ^{15}N pyridine in methanol[30] and neat pyridine.[70]

For further optimization, it is reasonable to expect that large T_1, specifically, a T_1 that is large at the magnetic evolution field, will increase polarization levels. As reported in Table 2, benzonitrile stands out in terms of long T_1. Therefore, we tested benzonitrile at optimized concentrations. Figure 3B shows a buildup curve for benzonitrile where we find a relatively long buildup time constant of 40.8 s. Specifically, for this system we observe the highest hyperpolarization levels at a catalyst loading of 25 mol% (0.25 mM [IrCl(IMes)(COD)] activated in the presence of one catalyst equivalent of pyridine 0.25 mM and four catalyst equivalents ^{15}N-benzonitrile (1 mM)). Note that in absence of stabilizing coligand (pyridine) enhancements drop by ~50%. Large catalyst loading (c_{sub}/c_{cat} = 4) leads to high levels of polarization because a low excess of substrate increases the likelihood of a polarization event per substrate molecule; this is consistent with theoretical predictions by Barskiy et al.[67] and experimental findings by Appleby et al.[71]

On this system, we examined the influence of para-H$_2$ flow rate at maximized pressure (limited to 10 bar by the experimental setup) as depicted in Figure 3C. In the investigated range, hyperpolarization levels are linearly dependent on the flow rate—in line with previous studies.[70] At even higher flow rates the sample volume ($V_{bubbles} + V_{liquid}$) is larger than the homogeneous μT magnetic field region, and polarization levels drop. The highest polarization was obtained at 130 sccm at 10 bar of 85% para-H$_2$. We obtain 16% ^{15}N polarization as illustrated in Figure 3D. The results indicate that hyperpolarization levels are limited by the hydrogen exchange from gas to liquid phase; i.e., the interface area between bubbles and solution. We believe that improvements over the reported 16% are within reach by more efficient dispersion of para-H$_2$.

In summary, we propose the following sequence of experiments: First, optimization of magnetic field and temper-

ature, followed by a dilution series at a given c_{sub}/c_{cat} ratio to choose the best catalyst concentration c_{cat}. At the identified c_{cat}, substrate concentration should be optimized. Typically, we find that optimal c_{sub} is about 4 to 5 times c_{cat} such that the catalysts are coordinatively saturated but an excess of free substrate remains. Finally, para-H_2 pressure and flow should be chosen as high as possible for a given setup. We acknowledge that all parameters are interdependent such that multiple cycles through these optimization steps may lead to even higher hyperpolarization level.

CONCLUSION AND OUTLOOK

In this article we have shown that SABRE-SHEATH can hyperpolarize a wide range of nitrogen-containing compounds, often outside the reach of ^1H-SABRE. The presented results suggest that sp and sp^2 hybridized nitrogens can be hyperpolarized, and ^{15}N polarization of at least several percent can be obtained easily and rapidly (30 s to 1 min) if no impeding factors such as steric hindrance or proton exchange inhibit polarization buildup.[42,48,70]

Furthermore, we have shown that ^{15}N T_1 times may be extraordinarily long and can in special cases exceed 10 min. We obtain extended relaxation times at relatively low magnetic fields of 1 T, using a permanent magnet-based spectrometer. The results are contrasted to measurements at 8.5 T where one may observe only slightly higher S/N ($\sim$3) if relaxation delays are neglected. The extended T_1 times at low field quickly compensate for the S/N losses when tracking hyperpolarized species on longer time scales. Moreover, the demonstrated hyperpolarization levels allow for ^{15}N imaging[30,72,73] (likely even in low magnetic fields). The cited demonstrations show images with 2×2 mm^2 resolution acquired in less than a second.[30]

In addition, polarization transfer strategies from ^{15}N to ^1H have been developed avoiding detection on the low gyromagnetic ratio ^{15}N for read-out.[74−77] Such polarization transfer strategies may increase S/N by another order of magnitude.

Finally, we present a systematic strategy to optimize SABRE-SHEATH experiments for maximum hyperpolarization. The sequence consists of optimization of temperature and μT magnetic fields, a dilution series to determine the optimal catalyst concentration, and use of high para-H_2 pressure and flow.

The present contribution elucidates upon the interplay of kinetic parameters and system compositions, as well as extrinsic parameters on the polarization levels. This is a significant stepping stone for optimization of heterogeneous SABRE,[78,79] SABRE in biocompatible aqueous media,[80−83] and modes to continuously supply polarized substrates. Such advances, in combination with low-cost, low-field MRI, let us envision hyperpolarized biomolecular MRI in the near future.

ASSOCIATED CONTENT

⊙ Supporting Information

The Supporting Information is available free of charge on the ACS Publications website at DOI: 10.1021/acs.jpcc.6b12097.

Detailed descriptions of 1) Characteristics of chemical exchange, 2) Experimental determination of complex lifetimes, 3) Hyperpolarization Transfer Theory, 4) Experimental Details, and 5) Spectral data and miscellaneous information (PDF)

Video showing the experimental procedure (AVI)

AUTHOR INFORMATION

Corresponding Authors
*E-mail: thomas.theis@duke.edu.
*E-mail: warren.warren@duke.edu.

ORCID ⊙
Johannes F. P. Colell: 0000-0001-9020-344X
Danila A. Barskiy: 0000-0002-2819-7584
Qiu Wang: 0000-0002-6803-9556
Steven J. Malcolmson: 0000-0003-3229-0949
Eduard Y. Chekmenev: 0000-0002-8745-8801
Thomas Theis: 0000-0001-6779-9978

Author Contributions
All authors have given approval to the final version of the manuscript.

Notes
The authors declare no competing financial interest.

ABBREVIATIONS

SABRE: Signal Amplification by Reversible Exchange
SHEATH: Shield Enables Alignment Transfer to Hetero-nuclei
para-H_2: para-hydrogen
PHIP: para-hydrogen-induced polarization
CSA: Chemical Shift Anisotropy
CHCA: α-Cyano-4-hydroxycinnamic acid
S/N: signal-to-noise ratio
SI: Supporting Information
MRI: Magnetic Resonance Imaging
NMR: Nuclear Magnetic Resonance
rms: root-mean-square

REFERENCES

(1) Ardenkjaer-Larsen, J. H.; Fridlund, B.; Gram, A.; Hansson, G.; Hansson, L.; Lerche, M. H.; Servin, R.; Thaning, M.; Golman, K. Increase in signal-to-noise ratio of > 10,000 times in liquid-state NMR. *Proc. Natl. Acad. Sci. U. S. A.* **2003**, *100*, 10158−10163.
(2) Nikolaou, P.; Coffey, A. M.; Barlow, M. J.; Rosen, M.; Goodson, B. M.; Chekmenev, E. Y. Temperature-Ramped ^{129}Xe Spin Exchange Optical Pumping. *Anal. Chem.* **2014**, *86*, 8206−8212.
(3) Griffin, R. G.; Prisner, T. F. High field dynamic nuclear polarization-the renaissance. *Phys. Chem. Chem. Phys.* **2010**, *12*, 5737−5740.
(4) Ardenkjaer-Larsen, J.-H.; Boebinger, G. S.; Comment, A.; Duckett, S.; Edison, A. S.; Engelke, F.; Griesinger, C.; Griffin, R. G.; Hilty, C.; Maeda, H.; et al. Facing and Overcoming Sensitivity Challenges in Biomolecular NMR Spectroscopy. *Angew. Chem., Int. Ed.* **2015**, *54*, 9162−9185.
(5) Walker, T. G.; Happer, W. Spin-exchange optical pumping of noble-gas nuclei. *Rev. Mod. Phys.* **1997**, *69*, 629−642.

(6) Freeman, M. S.; Emami, K.; Driehuys, B. Characterizing and modeling the efficiency limits in large-scale production of hyperpolarized ^{129}Xe. *Phys. Rev. A: At., Mol., Opt. Phys.* **2014**, *90*, 023406.

(7) Chen, W. C.; Gentile, T. R.; Ye, Q.; Walker, T. G.; Babcock, E. On the limits of spin-exchange optical pumping of ^{3}He. *J. Appl. Phys.* **2014**, *116*, 014903.

(8) Barskiy, D. A.; Coffey, A. M.; Nikolaou, P.; Mikhaylov, D. M.; Goodson, B. M.; Branca, R. T.; Lu, G. J.; Shapiro, M. G.; Telkki, V.-V.; Zhivonitko, V. V.; et al. NMR Hyperpolarization Techniques of Gases. *Chem. - Eur. J.* **2017**, *23*, 725−751.

(9) Zheng, Y.; Miller, G. W.; Tobias, W. A.; Cates, G. D. A method for imaging and spectroscopy using γ-rays and magnetic resonance. *Nature* **2016**, *537*, 652−655.

(10) Ward, H. R.; Lawler, R. G. Nuclear magnetic resonance emission and enhanced absorption in rapid organometallic reactions. *J. Am. Chem. Soc.* **1967**, *89*, 5518−5519.

(11) Kaptein, R. Chemically induced dynamic nuclear polarization in five alkyl radicals. *Chem. Phys. Lett.* **1968**, *2*, 261−267.

(12) Hermkens, N. K. J.; Eshuis, N.; van Weerdenburg, B. J. A.; Feiters, M. C.; Rutjes, F. P. J. T.; Wijmenga, S. S.; Tessari, M. NMR-Based Chemosensing via pH$_2$ Hyperpolarization: Application to Natural Extracts. *Anal. Chem.* **2016**, *88*, 3406−3412.

(13) Eshuis, N.; van Weerdenburg, B. J. A.; Feiters, M. C.; Rutjes, F. P. J. T.; Wijmenga, S. S.; Tessari, M. Quantitative Trace Analysis of Complex Mixtures Using SABRE Hyperpolarization. *Angew. Chem., Int. Ed.* **2015**, *54*, 1372−1372.

(14) Eshuis, N.; Aspers, R. L. E. G.; van Weerdenburg, B. J. A.; Feiters, M. C.; Rutjes, F. P. J. T.; Wijmenga, S. S.; Tessari, M. 2D NMR Trace Analysis by Continuous Hyperpolarization at High Magnetic Field. *Angew. Chem., Int. Ed.* **2015**, *54*, 14527−14530.

(15) Eshuis, N.; Hermkens, N.; van Weerdenburg, B. J. A.; Feiters, M. C.; Rutjes, F. P. J. T.; Wijmenga, S. S.; Tessari, M. Toward Nanomolar Detection by NMR Through SABRE Hyperpolarization. *J. Am. Chem. Soc.* **2014**, *136*, 2695−2698.

(16) Rodrigues, T. B.; Serrao, E. M.; Kennedy, B. W.; Hu, D. E.; Kettunen, M. I.; Brindle, K. M. Magnetic resonance imaging of tumor glycolysis using hyperpolarized 13C-labeled glucose. *Nat. Med.* **2014**, *20*, 93−7.

(17) Nelson, S. J.; Kurhanewicz, J.; Vigneron, D. B.; Larson, P. E.; Harzstark, A. L.; Ferrone, M.; van Criekinge, M.; Chang, J. W.; Bok, R.; Park, I.; et al. Metabolic imaging of patients with prostate cancer using hyperpolarized [1-(13)C]pyruvate. *Sci. Transl. Med.* **2013**, *5*, 198ra108.

(18) Keshari, K. R.; Wilson, D. M. Chemistry and biochemistry of ^{13}C hyperpolarized magnetic resonance using dynamic nuclear polarization. *Chem. Soc. Rev.* **2014**, *43*, 1627−59.

(19) Keshari, K. R.; Wilson, D. M.; Sai, V.; Bok, R.; Jen, K.-Y.; Larson, P.; Van Criekinge, M.; Kurhanewicz, J.; Wang, Z. J. Non-invasive in vivo imaging of diabetes-induced renal oxidative stress and response to therapy using hyperpolarized ^{13}C dehydroascorbate magnetic resonance. *Diabetes* **2015**, *64*, 344.

(20) Merritt, M. E.; Harrison, C.; Sherry, A. D.; Malloy, C. R.; Burgess, S. C. Flux through hepatic pyruvate carboxylase and phosphoenolpyruvate carboxykinase detected by hyperpolarized 13C magnetic resonance. *Proc. Natl. Acad. Sci. U. S. A.* **2011**, *108*, 19084−9.

(21) Adams, R. W.; Aguilar, J. A.; Atkinson, K. D.; Cowley, M. J.; Elliott, P. I. P.; Duckett, S. B.; Green, G. G. R.; Khazal, I. G.; Lopez-Serrano, J.; Williamson, D. C. Reversible Interactions with para-Hydrogen Enhance NMR Sensitivity by Polarization Transfer. *Science* **2009**, *323*, 1708−1711.

(22) Eisenschmid, T. C.; Kirss, R. U.; Deutsch, P. P.; Hommeltoft, S. I.; Eisenberg, R.; Bargon, J.; Lawler, R. G.; Balch, A. L. Para Hydrogen Induced Polarization in Hydrogenation Reactions. *J. Am. Chem. Soc.* **1987**, *109*, 8089−8091.

(23) Golman, K.; Axelsson, O.; Johannesson, H.; Mansson, S.; Olofsson, C.; Petersson, J. S. Parahydrogen-induced polarization in imaging: Subsecond C-13 angiography. *Magn. Reson. Med.* **2001**, *46*, 1−5.

(24) Bowers, C. R.; Weitekamp, D. P. Parahydrogen and synthesis allow dramatically enhanced nuclear alignment. *J. Am. Chem. Soc.* **1987**, *109*, 5541−5542.

(25) Bowers, C. R.; Weitekamp, D. P. Transformation of Symmetrization Order to Nuclear-Spin Magnetization by Chemical Reaction and Nuclear Magnetic Resonance. *Phys. Rev. Lett.* **1986**, *57*, 2645−2648.

(26) Hövener, J.-B.; Knecht, S.; Schwaderlapp, N.; Hennig, J.; von Elverfeldt, D. Continuous Re-hyperpolarization of Nuclear Spins Using Parahydrogen: Theory and Experiment. *ChemPhysChem* **2014**, *15*, 2451−2457.

(27) Nikolaou, P.; Goodson, B. M.; Chekmenev, E. Y. NMR Hyperpolarization Techniques for Biomedicine. *Chem. - Eur. J.* **2015**, *21*, 3156−3166.

(28) Cowley, M. J.; Adams, R. W.; Atkinson, K. D.; Cockett, M. C. R.; Duckett, S. B.; Green, G. G. R.; Lohman, J. A. B.; Kerssebaum, R.; Kilgour, D.; Mewis, R. E. Iridium N-Heterocyclic Carbene Complexes as Efficient Catalysts for Magnetization Transfer frompara-Hydrogen. *J. Am. Chem. Soc.* **2011**, *133*, 6134−6137.

(29) Theis, T.; Truong, M. L.; Coffey, A. M.; Shchepin, R. V.; Waddell, K. W.; Shi, F.; Goodson, B. M.; Warren, W. S.; Chekmenev, E. Y. Microtesla SABRE Enables 10% Nitrogen-15 Nuclear Spin Polarization. *J. Am. Chem. Soc.* **2015**, *137*, 1404−1407.

(30) Truong, M. L.; Theis, T.; Coffey, A. M.; Shchepin, R. V.; Waddell, K. W.; Shi, F.; Goodson, B. M.; Warren, W. S.; Chekmenev, E. Y. ^{15}N Hyperpolarization by Reversible Exchange Using SABRE-SHEATH. *J. Phys. Chem. C* **2015**, *119*, 8786−8797.

(31) Zhivonitko, V. V.; Skovpin, I. V.; Koptyug, I. V. Strong ^{31}P nuclear spin hyperpolarization produced via reversible chemical interaction with parahydrogen. *Chem. Commun.* **2015**, *51*, 2506−2509.

(32) Fleming, F. F.; Yao, L.; Ravikumar, P. C.; Funk, L.; Shook, B. C. Nitrile-Containing Pharmaceuticals: Efficacious Roles of the Nitrile Pharmacophore. *J. Med. Chem.* **2010**, *53*, 7902−7917.

(33) Mewis, R. E.; Green, R. A.; Cockett, M. C. R.; Cowley, M. J.; Duckett, S. B.; Green, G. G. R.; John, R. O.; Rayner, P. J.; Williamson, D. C. Strategies for the Hyperpolarization of Acetonitrile and Related Ligands by SABRE. *J. Phys. Chem. B* **2015**, *119*, 1416−1424.

(34) Wang, H.; Lanks, K. W. 2-Cyanocinnamic Acid Sensitization of L929 Cells to Killing by Hyperthermia. *Cancer research* **1986**, *46*, 5349−5352.

(35) Barskiy, D. A.; Shchepin, R. V.; Coffey, A. M.; Theis, T.; Warren, W. S.; Goodson, B. M.; Chekmenev, E. Y. Over 20% ^{15}N Hyperpolarization in Under One Minute for Metronidazole, an Antibiotic and Hypoxia Probe. *J. Am. Chem. Soc.* **2016**, *138*, 8080−8083.

(36) Halestrap, A. P.; Denton, R. M. Specific inhibition of pyruvate transport in rat liver mitochondria and human erythrocytes by α-cyano-4-hydroxycinnamate. *Biochem. J.* **1974**, *138*, 313−316.

(37) Morais-Santos, F.; Miranda-Goncalves, V.; Pinheiro, S.; Vieira, A. F.; Paredes, J.; Schmitt, F. C.; Baltazar, F.; Pinheiro, C. Differential sensitivities to lactate transport inhibitors of breast cancer cell lines. *Endocr.-Relat. Cancer* **2014**, *21*, 27−38.

(38) McKeage, K. Alectinib: A Review of Its Use in Advanced ALK-Rearranged Non-Small Cell Lung Cancer. *Drugs* **2015**, *75*, 75−82.

(39) Santarpia, M.; Altavilla, G.; Rosell, R. Alectinib: a selective, next-generation ALK inhibitor for treatment of ALK-rearranged non-small-cell lung cancer. *Expert Rev. Respir. Med.* **2015**, *9*, 255−268.

(40) Conti, P.; Tamborini, L.; Pinto, A.; Blondel, A.; Minoprio, P.; Mozzarelli, A.; De Micheli, C. Drug Discovery Targeting Amino Acid Racemases. *Chem. Rev.* **2011**, *111*, 6919−6946.

(41) Eliot, A. C.; Kirsch, J. F. Pyridoxalphophateenzymes: Mechanistic, Structural, and Evolutionary Considerations. *Annu. Rev. Biochem.* **2004**, *73*, 383−415.

(42) Logan, A. W.; Theis, T.; Colell, J. F.; Warren, W. S.; Malcolmson, S. J. Hyperpolarization of Nitrogen-15 Schiff Bases by Reversible Exchange Catalysis with para-Hydrogen. *Chem. - Eur. J.* **2016**, *22*, 10777−81.

(43) Feng, Y.; Theis, T.; Wu, T.-L.; Claytor, K.; Warren, W. S. Long-lived polarization protected by symmetry. *J. Chem. Phys.* **2014**, *141*, 134307.

(44) Ellinger, P.; Kader, M. M. A. Nicotinamide metabolism in mammals. *Biochem. J.* **1949**, *44*, 77–87.

(45) Cantó, C.; Houtkooper; Riekelt, H.; Pirinen, E.; Youn; Dou, Y.; Oosterveer; Maaike, H.; Cen, Y.; Fernandez-Marcos; Pablo, J.; Yamamoto, H.; Andreux; Pénélope, A.; Cettour-Rose, P.; et al. The NAD+ Precursor Nicotinamide Riboside Enhances Oxidative Metabolism and Protects against High-Fat Diet-Induced Obesity. *Cell Metab.* **2012**, *15*, 838–847.

(46) Sauve, A. A. NAD+ and vitamin B3: from metabolism to therapies. *J. Pharmacol. Exp. Ther.* **2008**, *324*, 883–893.

(47) Shchepin, R. V.; Barskiy, D. A.; Mikhaylov, D. M.; Chekmenev, E. Y. Efficient Synthesis of Nicotinamide-1−^{15}N for Ultrafast NMR Hyperpolarization Using Parahydrogen. *Bioconjugate Chem.* **2016**, *27*, 878–882.

(48) Shchepin, R. V.; Barskiy, D. A.; Coffey, A. M.; Theis, T.; Shi, F.; Warren, W. S.; Goodson, B. M.; Chekmenev, E. Y. ^{15}N Hyperpolarization of Imidazole-^{15}N$_2$ for Magnetic Resonance pH Sensing Via SABRE-SHEATH. *ACS Sens.* **2016**, *1*, 640.

(49) Hartley, G. S. The Cis-form of Azobenzene. *Nature* **1937**, *140*, 281–281.

(50) Merino, E.; Ribagorda, M. Control over molecular motion using thecis−transphotoisomerization of the azo group. *Beilstein J. Org. Chem.* **2012**, *8*, 1071–1090.

(51) Bohle, D. S.; Rosadiuk, K. A. Nitric Oxide Catalysis of Diazene E/Z Isomerization. *Inorg. Chem.* **2015**, *54*, 7145–7151.

(52) Theis, T.; Ortiz, G. X.; Logan, A. W. J.; Claytor, K. E.; Feng, Y.; Huhn, W. P.; Blum, V.; Malcolmson, S. J.; Chekmenev, E. Y.; Wang, Q.; et al. Direct and cost-efficient hyperpolarization of long-lived nuclear spin states on universal ^{15}N$_2$-diazirine molecular tags. *Sci. Adv.* **2016**, *2*, e1501438.

(53) Abragam, A. *The principles of nuclear magnetism*; Clarendon Press: Oxford, 1961.

(54) Hoult, D. I.; Richards, R. E. The signal-to-noise ratio of the nuclear magnetic resonance experiment. *J. Magn. Reson.* **1976**, *24*, 71–85.

(55) Hoult, D. I.; Lauterbur, P. C. The sensitivity of the zeugmatographic experiment involving human samples. *J. Magn. Reson.* **1979**, *34*, 425–433.

(56) Hoult, D. I. Sensitivity of the NMR Experiment. In *eMagRes.*; John Wiley & Sons, Ltd: 2007.

(57) Hoult, D. I.; Richards, R. E. The signal-to-noise ratio of the nuclear magnetic resonance experiment. *J. Magn. Reson.* **1976**, *24*, 71–85.

(58) Hoult, D. I. Sensitivity of Whole Body MRI Experiments. *Enc. Magn. Reson.* **2007**, DOI: 10.1002/9780470034590.emrstm0491.

(59) Minard, K. R.; Wind, R. A. Solenoidal microcoil design—Part II: Optimizing winding parameters for maximum signal-to-noise performance. *Concepts Magn. Reson.* **2001**, *13*, 190–210.

(60) Danieli, E.; Perlo, J.; Blümich, B.; Casanova, F. Highly Stable and Finely Tuned Magnetic Fields Generated by Permanent Magnet Assemblies. *Phys. Rev. Lett.* **2013**, *110*, 180801.

(61) Sarracanie, M.; LaPierre, C. D.; Salameh, N.; Waddington, D. E. J.; Witzel, T.; Rosen, M. S. Low-Cost High-Performance MRI. *Sci. Rep.* **2015**, *5*, 15177.

(62) Suefke, M.; Liebisch, A.; Blumich, B.; Appelt, S. External high-quality-factor resonator tunes up nuclear magnetic resonance. *Nat. Phys.* **2015**, *11*, 767–771.

(63) Coffey, A. M.; Truong, M.; Chekmenev, E. Y. Low-field MRI can be more sensitive than high-field MRI. *J. Magn. Reson.* **2013**, *237*, 169–174.

(64) Hata, R.; Nonaka, H.; Takakusagi, Y.; Ichikawa, K.; Sando, S. Design of a hyperpolarized ^{15}N NMR probe that induces a large chemical-shift change upon binding of calcium ions. *Chem. Commun.* **2015**, *51*, 12290–12292.

(65) Clavijo Jordan, M. V.; Lo, S.-T.; Chen, S.; Preihs, C.; Chirayil, S.; Zhang, S.; Kapur, P.; Li, W.-H.; De Leon-Rodriguez, L. M.; Lubag,

A. J. M.; et al. Zinc-sensitive MRI contrast agent detects differential release of Zn(II) ions from the healthy vs. malignant mouse prostate. *Proc. Natl. Acad. Sci. U. S. A.* **2016**, *113*, E5464–E5471.

(66) Knecht, S.; Pravdivtsev, A. N.; Hövener, J.-B.; Yurkovskaya, A. V.; Ivanov, K. L. Quantitative description of the SABRE process: rigorous consideration of spin dynamics and chemical exchange. *RSC Adv.* **2016**, *6*, 24470–24477.

(67) Barskiy, D. A.; Pravdivtsev, A. N.; Ivanov, K. L.; Kovtunov, K. V.; Koptyug, I. V. Simple analytical model for Signal Amplification by Reversible Exchange (SABRE) process. *Phys. Chem. Chem. Phys.* **2016**, *18*, 89–93.

(68) Cowley, M. J.; Adams, R. W.; Atkinson, K. D.; Cockett, M. C. R.; Duckett, S. B.; Green, G. G. R.; Lohman, J. A. B.; Kerssebaum, R.; Kilgour, D.; Mewis, R. E. Iridium N-Heterocyclic Carbene Complexes as Efficient Catalysts for Magnetization Transfer from para-Hydrogen. *J. Am. Chem. Soc.* **2011**, *133*, 6134–6137.

(69) Günther, H. *NMR Spectroscopy: Basic Principles, Concepts and Applications in Chemistry*, 3rd ed.; Wiley-VCH: Weinheim, Germany, 2013.

(70) Shchepin, R. V.; Truong, M. L.; Theis, T.; Coffey, A. M.; Shi, F.; Waddell, K. W.; Warren, W. S.; Goodson, B. M.; Chekmenev, E. Y. Hyperpolarization of "Neat" Liquids by NMR Signal Amplification by Reversible Exchange. *J. Phys. Chem. Lett.* **2015**, *6*, 1961–1967.

(71) Appleby, K. M.; Mewis, R. E.; Olaru, A. M.; Green, G. G. R.; Fairlamb, I. J. S.; Duckett, S. B. Investigating pyridazine and phthalazine exchange in a series of iridium complexes in order to define their role in the catalytic transfer of magnetisation from para-hydrogen. *Chem. Sci.* **2015**, *6*, 3981–3993.

(72) Jiang, W.; Lumata, L.; Chen, W.; Zhang, S.; Kovacs, Z.; Sherry, A. D.; Khemtong, C. Hyperpolarized ^{15}N-pyridine Derivatives as pH-Sensitive MRI Agents. *Sci. Rep.* **2015**, *5*, 9104.

(73) Cudalbu, C.; Comment, A.; Kurdzesau, F.; van Heeswijk, R. B.; Uffmann, K.; Jannin, S.; Denisov, V.; Kirik, D.; Gruetter, R. Feasibility of in vivo ^{15}N MRS detection of hyperpolarized ^{15}N labeled choline in rats. *Phys. Chem. Chem. Phys.* **2010**, *12*, 5818–5823.

(74) Sarkar, R.; Comment, A.; Vasos, P. R.; Jannin, S.; Gruetter, R.; Bodenhausen, G.; Hall, H.; Kirik, D.; Denisov, V. P. Proton NMR of ^{15}N-Choline Metabolites Enhanced by Dynamic Nuclear Polarization. *J. Am. Chem. Soc.* **2009**, *131*, 16014–16015.

(75) Mishkovsky, M.; Cheng, T.; Comment, A.; Gruetter, R. Localized in vivo hyperpolarization transfer sequences. *Magn. Reson. Med.* **2012**, *68*, 349–352.

(76) Truong, M. L.; Coffey, A. M.; Shchepin, R. V.; Waddell, K. W.; Chekmenev, E. Y. Sub-second proton imaging of ^{13}C hyperpolarized contrast agents in water. *Contrast Media Mol. Imaging* **2014**, *9*, 333–341.

(77) Chekmenev, E. Y.; Norton, V. A.; Weitekamp, D. P.; Bhattacharya, P. Hyperpolarized ^{1}H NMR Employing Low γ Nucleus for Spin Polarization Storage. *J. Am. Chem. Soc.* **2009**, *131*, 3164–3165.

(78) Shi, F.; Coffey, A. M.; Waddell, K. W.; Chekmenev, E. Y.; Goodson, B. M. Heterogeneous Solution NMR Signal Amplification by Reversible Exchange. *Angew. Chem., Int. Ed.* **2014**, *53*, 7495–7498.

(79) Shi, F.; Coffey, A. M.; Waddell, K. W.; Chekmenev, E. Y.; Goodson, B. M. Nanoscale Catalysts for NMR Signal Enhancement by Reversible Exchange. *J. Phys. Chem. C* **2015**, *119*, 7525–7533.

(80) Shi, F.; He, P.; Best, Q.; Groome, K. A.; Truong, M. L.; Coffey, A. M.; Zimay, G.; Shchepin, R. V.; Waddell, K. W.; Chekmenev, E. Y.; et al. Aqueous NMR Signal Enhancement by Reversible Exchange in a Single Step Using Water-Soluble Catalysts. *J. Phys. Chem. C* **2016**, *120*, 12149.

(81) Zeng, H.; Xu, J.; McMahon, M. T.; Lohman, J. A. B.; van Zijl, P. C. M. Achieving 1% NMR polarization in water in less than 1 min using SABRE. *J. Magn. Reson.* **2014**, *246*, 119–121.

(82) Hövener, J.-B.; Schwaderlapp, N.; Borowiak, R.; Lickert, T.; Duckett, S. B.; Mewis, R. E.; Adams, R. W.; Burns, M. J.; Highton, L. A. R.; Green, G. G. R.; et al. Toward Biocompatible Nuclear Hyperpolarization Using Signal Amplification by Reversible Exchange: Quantitative in Situ Spectroscopy and High-Field Imaging. *Anal. Chem.* **2014**, *86*, 1767–1774.

(83) Truong, M. L.; Shi, F.; He, P.; Yuan, B.; Plunkett, K. N.; Coffey, A. M.; Shchepin, R. V.; Barskiy, D. A.; Kovtunov, K. V.; Koptyug, I. V.; et al. Irreversible Catalyst Activation Enables Hyperpolarization and Water Solubility for NMR Signal Amplification by Reversible Exchange. *J. Phys. Chem. B* **2014**, *118*, 13882−13889.